The Joint Institute for Nuclear Astrophysics

Measurement of low-energy resonances in the $^{19}F(\alpha,p)^{22}Ne$ reaction and their interpretation in terms of the R-matrix theory

C. Ugalde*, R. Azuma, A. Couture, J. Görres, H. Lee, E. Stech, E. Strandberg, W. Tan, and M. Wiescher.

University of Notre Dame

(Current address: Department of Physics and Astronomy, University of North Carolina, Chapel Hill, NC27599 and TUNL, Duke University, Durham, NC27708) .*

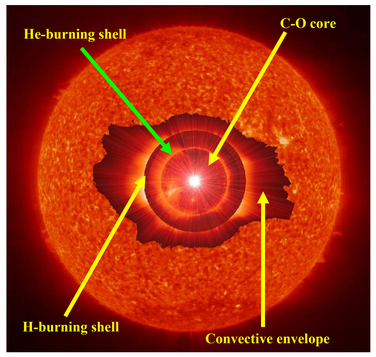

Figure 1. The structure of an AGB star (schematic).

The only stable isotope of fluorine,^{19}F , is by far the least abundant of stable nuclides in the 12-32 atomic-mass range in the solar system. Fluorine is fragile and can be destroyed easily by capturing protons at regular stellar temperatures. To make things more complicated, information on the abundance of fluorine is scarce as useful atomic lines are non-existent in the visible region of the spectrum. Nevertheless, fluorine has been identified in AGB stars. A schematic depiction of the structure of such a star is shown in Fig. 1.

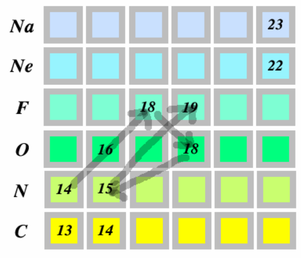

Figure 2. The reaction chain for fluorine production.

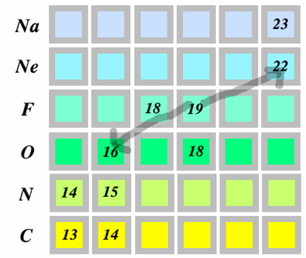

Figure 3. Reactions where fluorine is destroyed

The core of the star consists of an electron-degenerate mixture of carbon and oxygen. A shell of helium follows outwards; at the base of the shell helium is burning and once in a while the star pulsates and a convective zone is formed. It is here where fluorine is produced by the chain $^{14}N(\alpha,\gamma)^{18}F(\beta^+)^{18}O(p,\alpha)^{15}N(\alpha,\gamma)^{19}F$. (See Fig. 2.) Protons come from the reaction while neutrons are produced by . The protons required to form may be mixed down from outer layers of the star. Fluorine has to circumvent destruction and then move out across the convective envelope before we can observe it at the surface of the star. This is why it is of fundamental relevance to its synthesis to have a good determination of the rate at which it is destroyed. The main source of fluorine destruction is the reaction $^{19}F(\alpha,p)^{22}Ne$. (See Fig. 3.) The rate for the reaction holds large uncertainties. We have measured it in the laboratory with the 4 MV KN accelerator at The University of Notre Dame. (See Fig. 4.)

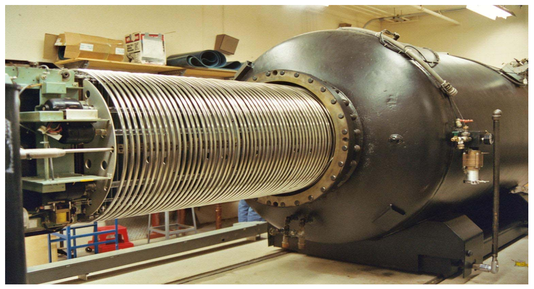

Figure 4. The 4 MV KN Van de Graaff accelerator at Notre Dame

In the first experiment, we measured the gamma yield from $^{19}F(\alpha,p\gamma)^{22}Ne$. The target was produced by evaporating CaF_2 onto a tantalum backing. A 55% Ge detector was used for alpha energies above 1.3 MeV while a BGO scintillator was used for the lower energies. The yield curve is shown below.

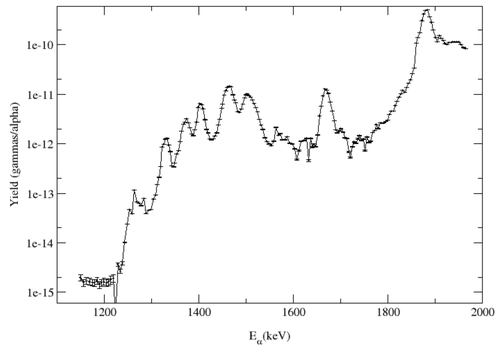

Figure 5. Gamma yield measured from the $^{19}F(\alpha,p_1\gamma)^{22}Ne$ reaction.

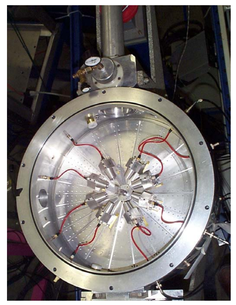

Figure 6. The Ortec scattering chamber.

In the second experiment, we measured both open channels (p_0 and p_1) of the $^{19}F(\alpha,p)^{22}Ne$ reaction. We prepared our target by evaporating CaF_2 onto a thin carbon foil. Si detectors were mounted around the target (see figure at left) at angles of 30°, 90°, 130° and 160°. Ni foils were mounted in front of each detector to stop scattered beam.

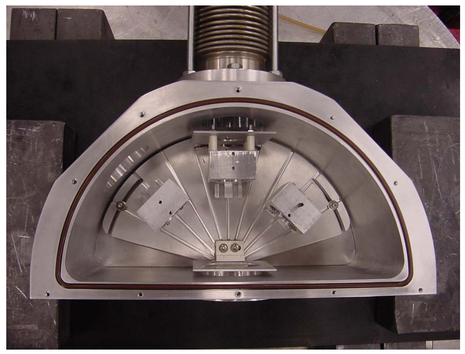

Figure 7. The solid target scattering chamber.

In a third experiment, we mounted two Si detectors very close to the target in order to maximize the solid angle. Both detectors were initially placed at 135° relative to the beam. Then we moved the detectors to 120° and 150° and measured excitation curves again. Finally, the yield curves were obtained by tilting the scattering chamber and target by 45° and mounting detectors at 75° and 105°. The chamber used is shown in figure 7 above while the data are shown in figure 8.

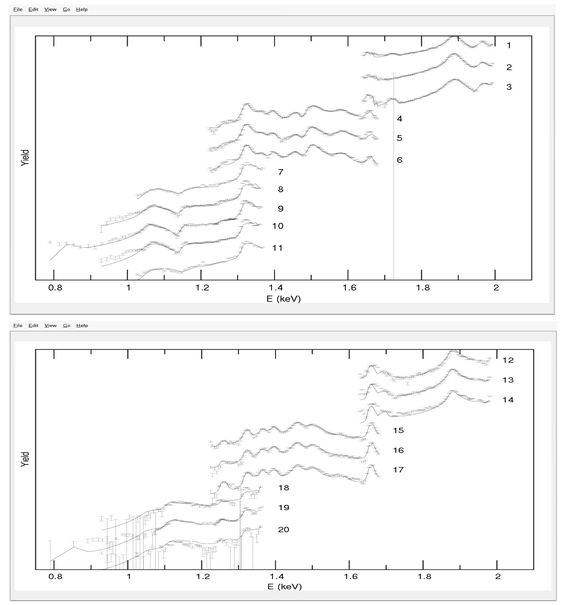

Figure 8. The experimental data and the R-matrix fits. The labels to the right of each curve are coded in table I.

Nuclear parameters such as the energy and widths of the resonances are required for estimating the reaction rate. The most reliable method for extracting them from the experimental data is the R-matrix formalism. Our experimental data have been analyzed with the new multichannel R-matrix code AZURE. The R-matrix fits are shown in figure 8.

Our version of the reaction rate is the first calculated for $^{19}F(\alpha,p)^{22}Ne$ from experimental results ever. It is shown compared to other theoretical and "in-use" rates in figure 9.

TABLE I: Summary of yield curves measured in this work

curve	reaction	angle	E_{min} (keV)	E_{max} (keV)	Δ(keV)
1	$^{19}F(\alpha,p_0)^{22}Ne$	130	1641	1993	15
2	$^{19}F(\alpha,p_0)^{22}Ne$	90	1641	1993	15
3	$^{19}F(\alpha,p_0)^{22}Ne$	30	1641	1993	15
4	$^{19}F(\alpha,p_0)^{22}Ne$	120	1224	1679	15
5	$^{19}F(\alpha,p_0)^{22}Ne$	100	1224	1679	15
6	$^{19}F(\alpha,p_0)^{22}Ne$	40	1224	1679	15
7	$^{19}F(\alpha,p_0)^{22}Ne$	105	1027	1367	25
8	$^{19}F(\alpha,p_0)^{22}Ne$	120	929	1359	35
9	$^{19}F(\alpha,p_0)^{22}Ne$	135	789	1363	25
10	$^{19}F(\alpha,p_0)^{22}Ne$	150	929	1359	35
11	$^{19}F(\alpha,p_0)^{22}Ne$	75	1027	1367	35
12	$^{19}F(\alpha,p_1)^{22}Ne$	130	1629	1981	15
13	$^{19}F(\alpha,p_1)^{22}Ne$	90	1629	1981	15
14	$^{19}F(\alpha,p_1)^{22}Ne$	30	1629	1981	15
15	$^{19}F(\alpha,p_1)^{22}Ne$	120	1224	1679	15
16	$^{19}F(\alpha,p_1)^{22}Ne$	100	1224	1679	15
17	$^{19}F(\alpha,p_1)^{22}Ne$	40	1224	1679	15
18	$^{19}F(\alpha,p_1)^{22}Ne$	120	929	1359	35
19	$^{19}F(\alpha,p_1)^{22}Ne$	135	789	1363	25
20	$^{19}F(\alpha,p_1)^{22}Ne$	150	929	1359	35

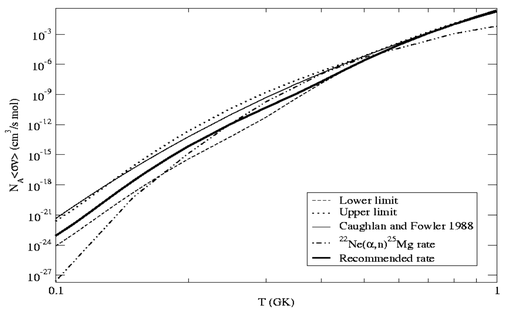

Figure 9. The rate of the $^{19}F(\alpha,p)^{22}Ne$ reaction.

This project is funded by the NSF through grant PHY0216783, and the Universities of JINA.